Thermal diffusion of a stiff rod-like mutant Y21M fd-virus

Pablo Blanco,* Hartmut Kriegs, M. Paul Lettinga, Peter Holmqvist, and Simone Wiegand*

Forschungszentrum Jülich GmbH, IFF - Soft Condensed Matter, D-52428 Jülich, Germany

E-mail: p.blanco@fz-juelich.de; s.wiegand@fz-juelich.de

*To whom correspondence should be addressed

Abstract

We investigated the thermal diffusion phenomena of a rod-like mutant filamentous *fd*-Y21M virus in the isotropic phase, by means of an improved infrared thermal diffusion forced Rayleigh scattering (IR-TDFRS) set-up crucial for measurements of slowly diffusing systems. Since this is the first thermal diffusion study of a stiff anisotropic solute, we investigate the influence of the shape anisotropy on the thermal diffusion behavior. The influence of temperature, *fd*-Y21M concentration and ionic strength in relation with the thermodiffusion properties is discussed. We characterize and eliminate the effect of these parameters on the absolute diffusion of the rods and show that diffusion determines the behavior of the Soret coefficient because the thermal diffusion coefficient is constant in the investigate regime. Our results indicate that for the thermal diffusion behavior structural changes of the surrounding water are more important than structural changes between the charged macroions. In the investigated temperature and concentration range, the *fd*-Y21M virus is thermophobic for the low salt content, while the solutions with the high salt content change from thermophobic to thermophilic behavior with decreasing the temperature. A comparison with recent measurements of other charged soft and biological matter systems shows that the shape anisotropy of the *fd*-virus becomes not visible in the results.

May 12, 2011

Introduction

Thermal diffusion, i.e. the mass transport caused by a temperature gradient, influences many processes. For instance, it has been shown that thermal diffusion influences magmatic differentiation,[1] convention in stars,[2] microstructure of the ocean,[3] biological transport,[4] analysis of protein interactions,[5] and is also considered in the context of the "*origin of life*"-question.[6] In the recent years the interest in thermal diffusion or thermophoresis in biological systems and also the transport of living matter in temperature gradients has increased. Mammalian spermatozoa responds to temperature gradients, so that it is guided in the female genital tract towards the egg.[7] This is also

known as thermotaxis and requires living sperms, so that it is not a pure thermophoretic process.

Recent simulations suggested that nucleotides and nucleic acid oligomers can be concentrated in prebiotic deep-sea alkaline vents by means of the thermal gradients originated between the warm volcanic rock and cold ocean water.[6] Lately, it has been experimentally demonstrated that protocells like vesicles can be concentrated in narrow channels with a thermogravitational configuration,[8] i.e., the thermal gradient is applied perpendicular to the gravity field into a vertical narrow cavity. It has also been shown that a micro thermal focusing field flow fractionation technique can be used to separate different bacterias.[9] Braun and coworkers demonstrated that thermal diffusion can trap DNA molecules,[10] and that DNA self replicates in a temperature gradient.[11] An all-optical microfluidic fluorescence method has been used to determine the thermal diffusion properties of DNA.[12,13] Recently, this method has been used to study the salt dependence in the thermal diffusion properties of single stranded DNA of up to 50 base pairs.[14] Although there has been a lot of activity in aqueous synthetic and biological systems, there are still many open questions. We still do not have a microscopic description which relates shape, size, charge and hydration shell of the molecules with the thermal diffusion behavior. It is known that sperm cells navigate from their cooler reservoir towards the warmer location of the egg, but the thermotaxis can only be observed as the sperms are active.[15] Apparently the forces in temperature gradients, which occur in living systems are different from the thermophoresis observed for colloidal particles. Looking at a virus is therefore the first step towards more biological systems.

In this study we investigate the thermal diffusion phenomena of a mutant filamentous bacteriophage *fd*-(Y21M). The wild type fd-viruses have been widely used as a robust colloidal model system, which is stable up to $T = 65\ ^{\circ}C$.[16] The main advantage of this systems is that they are rather monodisperse and have identical structures with same physical parameters such as mass, length and diameter.[17] They have been used[17–19] to test the validity of the statistical mechanical theory of Onsager[20] and its generalization to semiflexible chains made by Khokhlov and Semenov[21] to describe the isotropic nematic phase transition. It has also been used to study sedimentation processes of rod-like particles,[22] vorticity bending in suspensions of rod-like particles[23] and non-

equilibrium phase diagrams in electric field.[24] Recently, different *fd*-viruses have been chemically obtained with different surface properties that could help in studies of polyelectrolyte effects and liquid-crystaline phase behavior.[25]

The *fd*-Y21M is a natural rod-like particles of 910 nm length and diameter of 6.6 nm. They consist of a cylindrical shell composed of approximately 2700 copies of a major coat protein (50 amino acids in length) that encapsulates a circular single stranded DNA. In one end there are five copies of two minor proteins (genes 7 and 9) which are active in the initiation of the assembly of the virus, and in the other end there are another five copies of two proteins (genes 6 and 3) responsible of making up a host cell recognition complex.[26,27] The single-site mutant *fd*-Y21M is a more rigid rod compared to wild-type *fd*-Y21M virus. The persistence lengths of wild type and *fd*-Y21M are 2.8$\pm$0.7 μm and 9.9$\pm$0.7 μm, respectively.[19] They only differ by a single point mutation, where the amino acid methionine takes the place of tyrosine. Mutant *fd*-Y21M is with 910 nm slightly longer than the wild-type.[28]

We investigated the solutions of *fd*-Y21M in the isotropic phase by means of an improved infrared thermal diffusion forced Rayleigh scattering technique (IR-TDFRS),[29] in order to determine the thermal diffusion properties of slow diffusing systems, such as *fd*-Y21M virus. In order to have a workable signal to noise ratio we have to use relatively high concentrations of viruses however always in the isotropic. Also, we anticipate that the thermal diffusion is affected by the ionic strength, as bacteriophage *fd*-Y21M are polyelectrolytes. Therefore we performed our studies at high (110 mM ionic strength, *hs*) and low (1 mM ionic strength, *ls*) ionic strength. Because the absolute diffusion is influenced both by the ionic strength and concentration we first discuss these effects. For this we performed preliminary dynamic light scattering (DLS) experiments in order to compare collective diffusion results from both TDFRS and DLS. Then we focus on the temperature dependence of the thermal diffusion, D_{T} and Soret coefficients, S_{T}, of *fd*-Y21M. In the conclusion section we summerize our main results.

Experimental section

Sample Preparation

The *fd*-Y21M virus was grown and purified following standard biochemical protocols.[30] We used XL1-blue strain of *Escherichia coli* as the host bacteria cultured in a medium of tryptone (Fluka), yeast extract (Sigma) and NaCl (Merck). We prepared a batch of 6 L medium infected with bacterial colonies, where the virus is grown. The batch was first centrifuged for 30 minutes at 5180g in order to remove the bacteria. Then we added 2 wt% NaCl and 2 wt% polyethylene glycol (Aldrich) to precipitate the virus from the supernatant. After centrifugation for 30 mins at 5180g, the virus was collected and re-dispersed in a small amount of water. After this basic purification, the virus dispersions were purified by repeated centrifugations at 108800g for around 5 hours, and re-dispersions in the chosen buffer. Two different buffers of tris(hydroxymethyl)aminomethane (TRIS) were selected, one with low salt content (2 mM TRIS-HCl buffer adjusted to pH=8.2), and another one with higher salt content (20 mM TRIS-HCl + 100 mM NaCl buffer adjusted to pH=8.2). According to Kang *et al.*[31] the lower buffer concentration of 2 mM is still sufficient. They showed that, if the sample is exposed to CO_2 for a long time the pH value is reduced by less than 5% over time. In our experiments the TDFRS cells are sealed with a teflon stopper so that we do not expect a change in the pH.

Additionally, the virus was finally dialyzed against the chosen buffer. At the end, the virus suspension in the chosen buffer was stored at 5 °C. Prior **to** use, the virus was purified again by centrifugation at 5180g to remove potential bacteria.

Concentrations were obtained from UV absorbance measurements done with an UV-spectrometer (NanoDrop ND-1000, Peqlab). The optical density of *fd*-Y21M at 269 nm is 3.63 cm^{-1}.[19]

The contrast factor $(\partial n/\partial c)_{p,T}$ of the mixtures have been determined with an Anton Paar RXA 156 refractometer around the desired concentration ($\bar{c}$ ± 0.02) . The temperature control is $\Delta T = \pm 0.01$ K and the accuracy is $\Delta n = 0.00003$. The light source is a Sodium LED with a wavelength of 589.3$\pm$0.1 nm. In all cases, a linear dependence of the refractive index with mass

concentration was obtained. We found a constant value of $(\partial n/\partial c)_{p,T}$ = 0.197±0.002 for low salt buffer solutions, in the temperature range from 20 to 40 °C. In the case of higher salt buffer solutions, the value was $(\partial n/\partial c)_{p,T}$ = 0.203±0.001. These results are close to the values $(\partial n/\partial c)_{p,T}$ = 0.196±0.007 at 436 nm, and $(\partial n/\partial c)_{p,T}$ = 0.191±0.006 at 546 nm reported by Berkovitz and Day[32] of wild type *fd*-virus in KCl-P buffer.

A Michelson interferometer has been used to determine the refractive index increments with temperature, $(\partial n/\partial T)_{p,c}$, around the desired temperature (±2 K). The results show a constant value of $(\partial n/\partial T)_{p,c}$ = -1.469 10^{-4} K^{-1} at 40 °C, -1.209 10^{-4} K^{-1} at 30 °C, and -0.904 10^{-4} K^{-1} at 20 °C for low salt buffer solutions at different fd concentrations. In the case of higher salt buffer solutions, the values are slightly higher, $(\partial n/\partial T)_{p,c}$ = -1.480 10^{-4}, -1.232 10^{-4}, and -0.937 10^{-4} K^{-1}, at 40, 30 and 20 °C, respectively.

The samples were filtered through a non-pyrogenic sterile nylon filter of 5.0 μm before filling the optical quartz cells (Hellma) which are used in the IR-TDFRS experiments. The cells have an optical path length of 0.2 mm. The temperature in the sample cell is controlled by a thermostat ($\Delta T = \pm 0.1$ K), but the actual temperature in the sample is approximately 0.35K higher due to the heating by the IR laser at 980 nm. The experiments were repeated, at least, three times for each temperature and concentration.

Sample Characterization

In order to check that all experiments were in the isotropic phase, we characterized qualitatively the isotropic-nematic phase transition of *fd*-Y21M in both *hs* and *ls* buffers. In the experiment we placed *fd*-Y21M solutions of different concentrations between two crossed polarizers. We started from a high concentrated *fd*-Y21M solution and diluted the solution until we reached the isotropic phase. The object of this experiment is not to determine accurately the isotropic-nematic phase transition, but to select the range of *fd*-Y21M concentrations which are in the isotropic phase. In Figure 1 the results for the *ls* buffer are shown. As it can be observed, the isotropic-nematic phase transition is at around 3 mg/ml. Therefore, in order to be completely sure that we performed

the experiments in the isotropic phase, we decided to study the system at concentrations up to 2 mg/ml. In Figure 2, the results for the *hs* buffer are shown. In this case, the isotropic-nematic phase transition **is around** 13 mg/ml, which is in good agreement with the experimental value reported by Barry *et al.* of 13.9 mg/ml.[19]

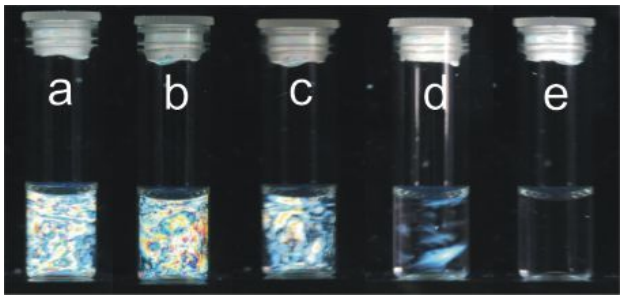

Figure 1: Isotropic-nematic phase transition for *fd*-Y21M in a 2mM Tris buffer at room temperature. a: 6.5 mg/ml, b: 5.2 mg/ml, c: 3.7 mg/ml, d: 3.0 mg/ml and e: 2.9 mg/ml. The images were taken between crossed polarizers.

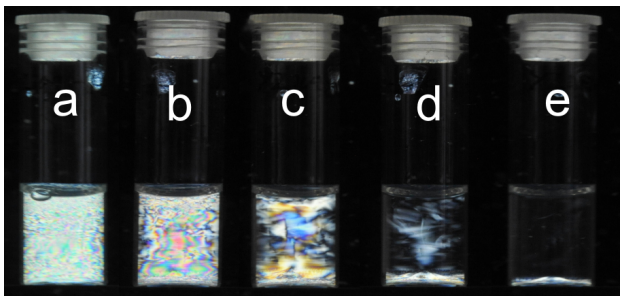

Figure 2: Isotropic-nematic phase transition for *fd*-Y21M in a 20mM Tris + 100 mM NaCl buffer at room temperature. a: 19.8 mg/ml, b: 15.0 mg/ml, c: 13.5 mg/ml, d: 13.1 mg/ml and e: 12.4 mg/ml. The images were taken between crossed polarizers.

Infrared Thermal Diffusion Forced Rayleigh Scattering

A detailed description of the thermal diffusion forced Rayleigh scattering technique can be found in the literature.[33–38] We used the infrared thermal diffusion forced Rayleigh scattering (IR-TDFRS) setup,[29] which is optimal for aqueous solutions. The main difference is that no dye is needed to convert the light energy into heat energy, due to the absorption of water at the wavelength of the infrared laser beam (λ_w=980 nm). Recently, this technique has been used to study the

transport properties in different aqueous systems of non-ionic surfactants[39,40] and of saccharide solutions.[41,42]

Summarizing what is explained in more detail in the above given references, the infrared laser beam is split into two beams that interfere in the sample cell, creating an intensity grating. The intensity grating is absorbed by the fluid and as a consequence, a temperature gradient builds up, which in turn causes a concentration grating by the effect of thermal diffusion. Both temperature and concentration gratings contribute to a combined refractive index grating which is read out by the Bragg diffraction of an He-Ne laser (λ_w=633 nm). The total heterodyne scattering intensity $\zeta_{\text{het}}(t)$ assuming an ideal excitation with a step function is given by

$$\zeta_{\text{het}}(t) = 1 - \exp\left(-\frac{t}{\tau_{\text{th}}}\right) - A\left(\tau - \tau_{\text{th}}\right)^{-1}\left\{\tau\left[1 - \exp\left(-\frac{t}{\tau}\right)\right] - \tau_{\text{th}}\left[1 - \exp\left(-\frac{t}{\tau_{\text{th}}}\right)\right]\right\} \quad (1)$$

with the steady state amplitude A

$$A = \left(\frac{\partial n}{\partial c}\right)_{p,T}\left(\frac{\partial n}{\partial T}\right)_{p,c}^{-1} S_{\text{T}} c\,(1-c) \quad (2)$$

where c is the mass concentration, τ_{th} the heat diffusion time, $(\partial n/\partial c)_{p,T}$ and $(\partial n/\partial T)_{p,c}$ are refractive index contrast factors in respect to mass concentration at constant pressure and temperature, and in respect to temperature at constant pressure and mass concentration, respectively. The Soret coefficient $S_{\text{T}} = D_{\text{T}}/D$ can be expressed as ratio of the thermal diffusion coefficient, D_{T}, and the collective diffusion coefficient, D. Whereas $D = 1/(q^2\tau)$ can be calculated from the diffusion time, τ, in Eq. (1) using q the magnitude of the grating vector which is given by

$$q = \frac{4\pi}{\lambda_w} sin\frac{\theta}{2} \quad (3)$$

where θ is the angle between the two writing beams at the wavelength λ_w. The transport coefficients are determined by fitting (Eq. (1)) to the measured heterodyne signal and deconvoluting the excitation function.[43,44]

We have modified the IR-TDFRS technique in order to improve the measurements of slow diffusing systems, such as *fd*-Y21M virus. A sketch of the IR-TDFRS setup is shown in Figure 3. The amelioration consist of two parts. First, the simultaneous record of the excitation function and diffracted signal (through the cell), so any external disturbance (thermal or mechanical) will affect both recorded signals in the same way. Secondly, the control of the grating position by the video camera, which assures a better stability of the grating for long term measurements. This has been achieved by replacing the original flip mirrors[29] in front of the cell and the camera, by a glass plate with a high transmission and a low reflectivity (10) and by a grey filter (12), respectively. Using a grey filter in front of the camera avoids ghost images on the camera due to internal reflections within the glass. For the phase synchronization of the excitation function we use a line grating, with the same period as the optical grating in its image plane (16). This line grating is mounted on a motorized translational stage. This can be moved perpendicular to the optical axis, so that the phase of the excitation function can be determined and adjusted. Using this additional grating reduces the noise in the determination of the phase. Simultaneously, also the camera measures the phase of the grating and a control loop is locking this phase for long time measurements by means of the piezo mirror (8), if this is necessary.

In Figure 4, we show two normalized heterodyne signals for a solution of 2 mg/ml *fd*-Y21M in a 2 mM TRIS buffer and in a 20 mM TRIS buffer plus 100 mM NaCl salt, respectively. The experimental data points (open symbols) are averaged over 2000 runs, and the lines are the fitted functions according to Eq. (1). It can be observed that the thermal plateau is reached after 0.1 ms. The concentration plateau is reached at 7 s for the *ls* solution with 2 mg/ml *fd*-Y21M, while for the *hs* solution with same *fd*-Y21M concentration, the equilibrium is reached after approximately 20 s. In the example with the *ls* buffer, the amplitude of the concentration plateau is positive, which means that the *fd*-Y21M virus goes to the cold and its S_T is positive. In contrast the amplitude of the concentration plateau is negative for the *hs* buffer, which implies that the *fd*-Y21M virus goes to the warm and its S_T is negative.

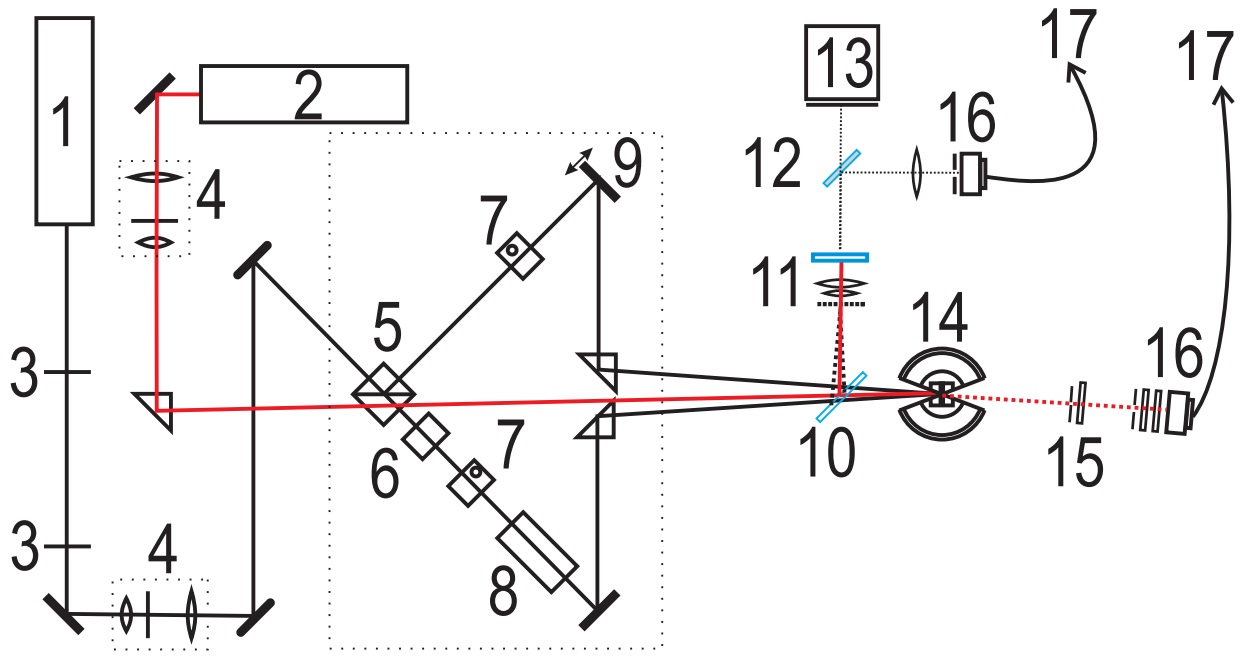

Figure 3: Sketch of the infrared TDFRS setup. (1) Infrared laser 980nm, (2) HeNe laser 633 nm, (3) pinhole, (4) spatial filter, (5) beam splitter, (6) $\lambda/2$ plate, (7) double Pockels cell, (8) piezo mirror, (9) Glan-Thompson polarizer, (10) glass plate with high transmission and low reflectivity, (11) infrared transmission filter and microscope objective with a reticle, (12) grey filter, (13) CCD camera, (14) sample cell holder, (15) filter, (16) grating on motorized stage with a lens, (17) mono mode fiber, and (18) avalanche diode (one to record the cell signal and another one to record the excitation function).

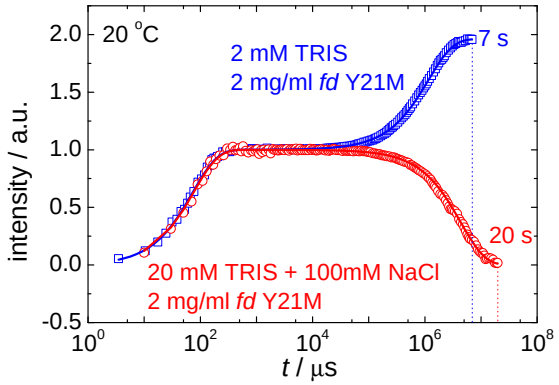

Figure 4: Normalized heterodyne signal for *fd*-Y21M in the studied two buffers with 2 mg/ml *fd*-Y21M concentration at 20 °C. The solid lines represent a fit of the experimental data to equation Eq. (1).

Results and Discussion

All experimental values obtained for S_T, D and D_T are listed in Table 1 and Table 2, for low salt (*ls*) and high salt (*hs*) solutions respectively. Figure 5 plots the results of thermal diffusion, collective diffusion and Soret coefficients as function of *fd*-Y21M concentration, for the different temperatures and concentrations.

Due to the complexity of the data we separate the discussion of the results of S_T, D and D_T. In the first two parts we focus on the effect of concentration and ionic strength. Then we focus on the effect of temperature for both buffered solutions.

Table 1: Thermal diffusion, collective mass diffusion and Soret coefficients of Y21M *fd*-virus at different concentrations and temperatures in a 2 mM TRIS-HCl buffer, pH=8.2.

fd concentration / mg ml^{-1}	temperature / °C	S_T / K^{-1}	D / 10^{-12} m^{2}s^{-1}	D_T / 10^{-12} m^{2}s^{-1}K^{-1}
0.5	40	0.999±0.004	5.58±0.14	5.59±0.13
	30	0.805±0.026	4.37±0.31	3.51±0.34
	20	0.518±0.038	3.36±0.38	1.75±0.32
1.0	40	0.682±0.007	9.14±0.58	6.25±0.35
	30	0.583±0.004	7.15±0.21	4.15±0.15
	20	0.401±0.020	5.65±0.03	2.27±0.12
2.0	40	0.385±0.006	14.9±1.29	5.73±0.43
	30	0.312±0.002	11.9±0.37	3.71±0.13
	20	0.220±0.005	9.65±0.17	2.13±0.06

fd-Y21M concentration influence

In Figure 5 the experimental results of thermal diffusion, collective diffusion and Soret coefficients are shown as function of *fd*-Y21M concentration. In *hs* and *ls* solutions, D_T remains constant, independent of the *fd*-Y21M concentration. This means that the tendency of *fd*-Y21M to go either to the cold or to the warm side is independent of the concentration in the solution. A similiar concentration dependence of D_T has also been found for polymers and colloids in the low concentration regime.[45,46] Typically it is expected that D_T decreases for higher concentration, but these concentration are certainly in the nematic regime of the *fd*-Y21M.

Table 2: Thermal diffusion, collective mass diffusion and Soret coefficients of Y21M *fd*-virus at different concentrations and temperatures in a 20 mM TRIS-HCl + 100 mM NaCl buffer, pH=8.2.

fd concentration / mg ml^{-1}	temperature / °C	S_T / K^{-1}	D / 10^{-12} m^{2}s^{-1}	D_T / 10^{-12} m^{2}s^{-1}K^{-1}
1.0	40	0.412±0.053	3.75±0.10	1.54±0.19
	30	0.148±0.006	2.72±0.16	0.40±0.04
	20	-0.261±0.043	2.08±0.28	-0.54±0.02
2.0	40	0.424±0.019	4.09±0.25	1.73±0.10
	30	0.133±0.001	3.73±0.14	0.50±0.02
	20	-0.243±0.018	2.51±0.22	-0.61±0.01
3.0	40	0.346±0.021	4.78±0.21	1.66±0.16
	30	0.116±0.006	4.19±0.34	0.48±0.04
	20	-0.197±0.018	2.96±0.18	-0.58±0.05

In *ls* solutions D increases with concentration for all investigated temperatures by a factor of 2.7-2.9, which depends slightly on the *fd*-Y21M concentration, while in *hs* solutions D increases by 30% with increasing *fd*-Y21M concentration. The reason is that in a system with repulsive interactions between particles, the collective diffusion increases with increasing particle concentration due to an increasing osmotic pressure.

At very low *fd*-Y21M concentrations, below the overlap concentration, c*, the self-diffusion coefficient should be equal to the collective or cooperative diffusion coefficient.[47] A direct comparison at these very low concentrations between DLS and TDFRS measurements was not possible, because the optical contrast in the TDFRS measurements was too low. Extrapolation of the preliminary data indicates that the DLS and TDFRS data approach each other. Future research and systematic DLS studies will have to identify the contribution of the dynamic structure factor at the fairly large scattering angles of $\theta \geq 20^\circ$ compared to $\theta = 3^\circ$ in the IR-TDFRS.

Regarding the Soret coefficient, in *ls* solutions S_T decreases with increasing *fd*-Y21M concentration, while for *hs* solutions it remains almost constant. This effect is only due to the change of D with *fd*-Y21M concentration as explained in the last paragraph, because D_T is independent of concentration.

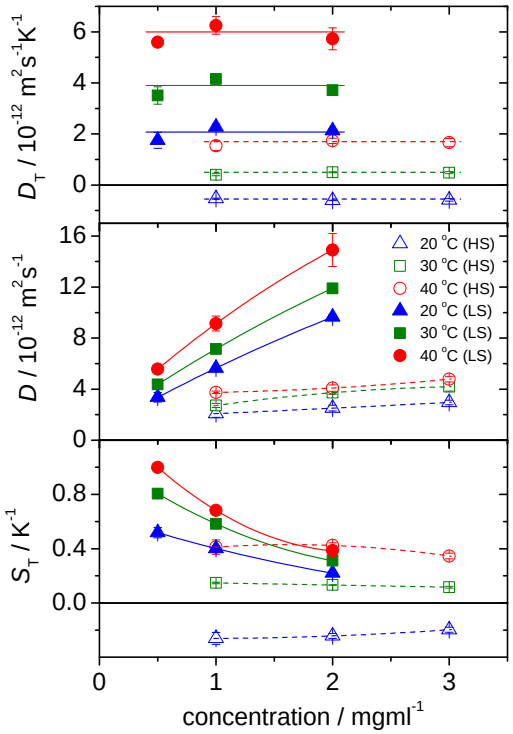

Figure 5: Concentration dependence of D_T, D and S_T coefficients of *fd*-Y21M at different temperatures and in two different buffers. Open symbols correspond to the high salt (*hs*) buffer of 20 mM Tris + 100 mM NaCl. Filled symbols correspond to the low salt (*ls*) buffer of 2 mM Tris.

Ionic strength dependence

The ionic strength, I, of the *ls* solution is 1 mM, but the addition of *fd*-Y21M to the solution increases I. Depending on the *fd*-Y21M concentration, I changes from 1.14 mM (c=0.5 mg/ml) to 1.55 mM (c=2.0 mg/ml). For that calculation we used a charge density per length of 10 e nm^{-1},[18,48] and a molecular weight of 1.64 10^7 g mol^{-1}. In *hs* solutions, I is 110-111 mM, where the contribution of *fd*-Y21M to the ionic strength is below 1%.

In the studied temperatures and *fd*-Y21M concentration range, the transport properties D and D_T show higher values for the low ionic strength solutions. The addition of salt to a charged system reduces the repulsive interactions between the particles. Therefore, an increase of the ionic strength leads to a slower collective diffusion, provided temperature and concentration are kept constant. Likewise, the increase of D with increasing *fd*-Y21M concentration is less pronounced in *hs* solutions. In very diluted solutions of *fd*-Y21M, D may be practically independent of the ionic strength.

Lower values of D are found in solutions with a higher salt content. This might be counter intuitive, because due to the larger Debye length of the macroions at low salt content their volume is larger than in the case of high salinity, so that they should diffuse faster in the later case. This holds for the long-time self diffusion coefficient,[49] but not for the collective diffusion coefficient, which can be expressed as $D(q) = D_0(H(q)/S(q))$ within the Smoluchowski dynamics of overdamped particle motion. The diffusion coefficient of an isolated particle is denoted as D_0, the hydrodynamic function as $H(q)$ and the static structure factor as $S(q)$. In the long wave length limit $S(q)$ can be approximated by $S(0) \equiv \lim_{q\to 0} S(q) = \rho_0 k_B T \chi_T$ and is proportional to the osmotic compressibility $\chi_T = 1/\rho_0 \, (\partial \rho_0 / \partial p) \, T$.[50] Due to the fact that the osmotic compressibility increases with increasing salt content the collective diffusion becomes smaller. The same observation has been made for apoferritin by Gapinski *et al.*[51] Only for very high volume fractions the situation might be inversed since then the hydrodynamic interactions dominate the behavior.[52]

Regarding the Soret coefficient, in general, an increase of the ionic strength decreases the value of S_T, although increasing temperature and *fd*-Y21M concentration makes the differences smaller.

A similar tendency of S_T with temperature, concentration and ionic strength dependence has also been found for lysozyme solutions.[53] Using the empirical equation Eq. (4), one could extrapolate the data to determine the sign change temperature for *ls* solutions, which would be at 8.2, 8.6 and 2.6 °C for *fd*-Y21M concentrations of 0.5 mg/ml, 1.0 mg/ml, and 2.0 mg/ml, respectively. Then, the Soret sign change temperature increases with increasing ionic strength. The knowledge of the temperature at which the Soret coefficient is zero is important from the point of view that any temperature disturbance in the system (small temperature gradients) will not create any *fd*-Y21M mass separation, and therefore *fd*-Y21M concentration will be homogeneous.

Recently, Ning *et al.*[54] showed that S_T of Ludox, polystyrene spheres,[13] and sodium dodecyl sulfate suspensions[55] increases as function of the Debye length, λ_{DH}. In the present study, in general, S_T of *fd*-Y21M also increases with λ_{DH}. The Debye length of *ls* solutions is between 7.7 nm and 9.0 nm at 20 °C, depending on the *fd*-Y21M concentration, whereas in *hs* solutions λ_{DH} is 0.9 nm. At high temperatures, 40 °C, the Soret coefficient is almost identical for *ls* and *hs* solutions with 2 mg/ml *fd*-Y21M concentration, although the Debye length has a difference of one order of magnitude.

Temperature influence

In Figure 6 the thermal diffusion, collective diffusion and Soret coefficients are shown as function of the temperature. All three properties, D_T, D and S_T, increase with increasing temperature.

In *ls* solutions, D_T is always positive in the studied range of temperatures, which means that *fd*-Y21M moves to the cold side. To some extent the temperature dependence of D_T is influenced by the viscosity change with temperature as it had also been observed by Stadelmaier and Köhler.[56] Additionally, changes in the interactions with temperature influence the thermal diffusion behavior. This becomes even more evident for the *hs* solutions, where D_T changes its sign around 26 °C. At temperatures below 26 °C, D_T is negative, meaning that *fd*-Y21M moves to the warm side, while at temperatures above 26 °C, D_T is positive, which means that *fd*-Y21M moves to the cold region. The physical mechanism of this sign change with temperature is not well understood, al-

though it has been observed for many aqueous systems, such as aqueous mono and oligosaccharide solutions,[41,42] aqueous polysaccharide solutions,[57] DNA,[13] proteins solutions[58] and polypeptide solutions.[59] A recent systematic study by Vigolo *et al.*[60] of aqueous sodiumdodecyl sulfate solutions with different salt content showed also the same trend and it turned out that the thermoelectric contribution was not correlated with the thermal diffusion behavior.

For the *fd*-Y21M in water we observe that the system becomes more thermophilic with decreasing temperature. It is reasonable to assume that the hydrogen bonds become also stronger with decreasing temperature.[61] This explains the sign change at lower temperatures, where the hydrogen bonds are stronger compared to higher temperatures. The addition of salt has a similiar effect as lowering the temperature. This induces a higher order in the inner and outer hydration cell around the ions and leads also to a lower D_T. So the reduction of the temperature as well as the addition of salt results in a higher structure of the water molecules, which leads to a more thermophilic behavior of the *fd*-Y21M virus. Also Vigolo *et al.*[60] observed a lowering of D_T with increasing salt content, but the attempt to correlate the thermoelectric contribution with the thermal diffusion behavior failed. The increasing salt content at constant *fd*-Y21M concentration as well as an increase of the temperature will decrease the structure between the rod-like particles.[62] Regarding these two aspects we do not find a correlation with the thermal diffusion coeffcient. While D_T increase with increasing temperature it decreases with increasing salt content. Therefore, we conclude that the structural changes of the solvent surrounding the solute particles have a larger influence on the thermal diffusion behavior than the interactions between the solute particles. This implies that the interparticle interactions, which are certainly present because all investigated concentrations are well above the overlap concentration, influence the dynamics of the solution, but are less important for the thermal diffusion behavior of the system. This finding confirms the importance of the solvent structure on the thermal diffusion behavior and coincides with an earlier finding for polyethylenoxid in ethanol/water mixture,[63] which shows a sign change of the thermal diffusion behavior of the polymer once the hydrogen structure of water breaks due to the added ethanol.

Considering the collective diffusion coefficient, as one can expect, it increases with increasing temperature due to the decreasing viscosity with increasing temperature. Keeping the temperature constant D decreases by approx. 60-70% due to the added salt, if we compare the *ls* and *hs* solutions at *fd*-Y21M concentration of 1-2 mg/ml.

As expected for this slow diffusing charged rod-like particle the determined Soret coefficients are almost three orders of magnitude larger than the values obtained for low molecular weight mixtures, but the values are comparable to other biopolymers such as DNA.[13] Although the Soret coefficient is fairly large, the expected concentration separation in our set-up, the IR-TDFRS, is only in the order of $\Delta c = 10^{-4}$mg/ml due to the small temperature difference in the order of $\Delta T = 100\mu$K.[29]

The increase of S_{T} with temperature is more pronounced for *hs* solutions compared to *ls* solutions. Nevertheless the change in the slope due to addition of the salt is comparable with other charged systems such as sodiumdodecyl sulfate micelles[60] and seems not to be influenced by the anisotropic shape of the virus. In *hs* solutions there is a sign change of S_{T} and the variation of S_{T} for different concentrations is less pronounced as in the case of *ls*. The temperature at which the sign change occurs is independent of the *fd*-Y21M concentration. At higher temperatures, the values of S_{T} of *hs* and *ls* solutions approach each other, to the point that at the *fd*-Y21M concentration of 2 mg/ml the Soret coefficient of *hs* solution is slightly higher than that of the *ls* solution.

Iacopini *et al.* suggested to describe temperature dependence of S_{T} by the following empirical equation[59]

$$S_{\mathrm{T}}(T) = S_{\mathrm{T}}^{\infty}\left[1 - \exp\left(\frac{T_{inv} - T}{T_0}\right)\right] \tag{4}$$

where S_{T}^{∞} represents a high-T thermophobic limit, T_{inv} is the temperature where S_{T} changes sign, and T_0 represents the strength of temperature effects.

More recently, it has been identified that a single master curve is obtained when rescaling the temperature to T_{inv} and S_{T} to S_{T}^{∞}.[60] Then Eq. (4) becomes

$$\frac{S_{\mathrm{T}}\left(\widetilde{T}\right)}{S_{\mathrm{T}}^{\infty}} = 1 - \exp[A(1-\widetilde{T})] \tag{5}$$

where $\widetilde{T} = T/T_{inv}$ and $A = T_{inv}/T_0$. Although there has been no physical picture developed for Eq. (4) and Eq. (5), they describe the experimental data reasonably well.

They found that for sodium dodecyl sulfate solutions, the experimental results fitted to Eq. (5), are independent of the ionic strength of the solution. In the present work we used two different buffers with different ionic strength, therefore we checked the validity of Eq. (5) for *fd*-Y21M virus. In Figure 7, the results, according to equation Eq. (5), of *fd*-Y21M for the solutions with *fd*-Y21M concentration of 1 mg/ml and 2 mg/ml are shown. Keeping the *fd*-Y21M concentration constant, the results fit quite well to Eq. (5). In addition to what Vigolo *et al.* pointed out,[60] that for a specific particle system there are only two free parameters, our results indicate that the mass concentration has to be constant. Otherwise, different values of A can be expected (cf Figure 7, $A = 15.1$ and $A = 6.6$ for *fd*-Y21M concentrations of 1 mg/ml and 2 mg/ml, respectively). Only for the low concentration our A-value agrees with that of Vigolo *et al.*[60]

Conclusion

The temperature, concentration and ionic strength dependence of the thermal diffusion behavior of mutant *fd*-Y21M virus has been studied. D_{T}, D and S_{T} increase with increasing temperature. In the studied range of temperatures and *fd*-Y21M concentrations the *fd*-Y21M virus changes its thermophoretic behavior in solutions with an ionic strength of 110 mM. At these quite high salt solutions, at temperatures below 26 °C, *fd*-Y21M is thermophilic, while above 26 °C it is thermophobic. Decreasing the ionic strength of the buffer leads to a Soret sign change at lower temperatures. In general, an increase of the ionic strength decreases the values of the thermal transport properties. Correlating the structural changes of the water and the macroions induced by the salt variation with the thermal diffusion behavior it turns out that the thermal diffusion behavior is influenced by the water structure change but not by the structural changes between the

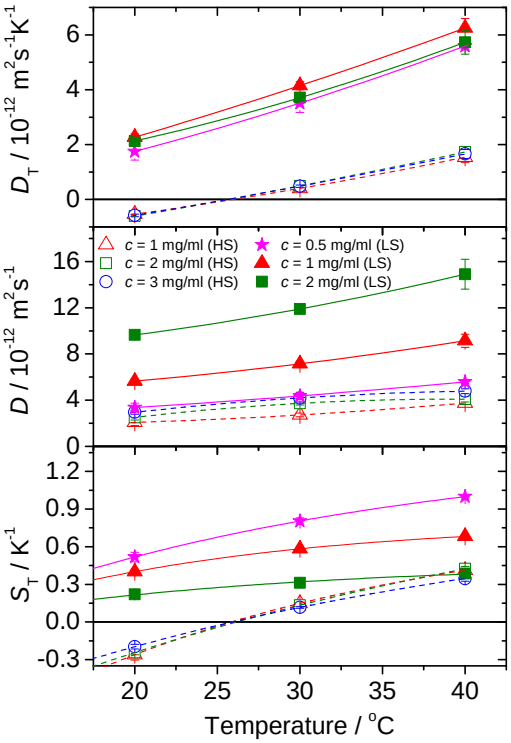

Figure 6: Temperature dependence of D_T, D and S_T coefficients of *fd*-Y21M at different concentrations and in two different buffers. Open symbols correspond to the high salt (*hs*) buffer of 20 mM Tris + 100 mM NaCl. Filled symbols correspond to the low salt (*ls*) buffer of 2 mM Tris.

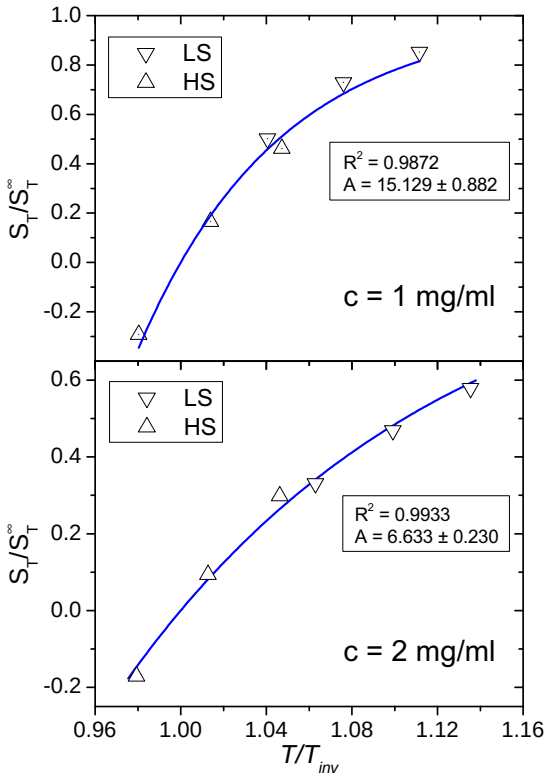

Figure 7: Temperature dependence of the Soret coefficient of *fd*-Y21M at 1 mg/ml (top plot) and 2 mg/ml (bottom plot) according to equation Eq. (5). *hs* and *ls* mean high salt and low salt solutions, respectively.

macroions. D_T is practically independent of the *fd*-Y21M concentration, while D increases with increasing *fd*-Y21M concentration, specially in low ionic strength solutions. This is due to the fact that *fd*-Y21M is an interacting system with repulsive interactions between the *fd*-Y21M viruses, and therefore D will increase with increasing the *fd*-Y21M concentration, and will decrease with increasing the ionic strength of the buffer. In both cases this is a free volume effect. If the salt content is low, the interactions are long ranged, so that the movement is restricted and also an increase of the *fd*-Y21M virus concentration leads to a reduced free volume.

The suitability of the thermal diffusion forced Rayleigh scattering technique to study such slow diffusing systems is underlined. So far we do not see an influence of the rod-like shape of the *fd*-Y21M virus on the thermal diffusion properties. For instance we see also an increase of S_T with increasing Debye length as it has been observed for spherical Ludox particles.[54] Further we saw, that the empirical equation Eq. (5) works for these rod-like particles. Here we would like to point out that changing the concentration of the particles leads to a different parameter set. Finally, we can conclude that the rod-like virus *fd*-Y21M behaves as colloidal or polymeric model system. We did not find a signature of the anisotropy nor of the virus character in the thermal diffusion behavior.

Acknowledgement

We appreciate many fruitful discussions with Johan Buitenhuis, Jan Dhont and Gerhard Nägele. We thank the Department of Education, Universities and Investigation of Basque Government for the grant BFI08188.0. Financial support due to the Deutsche Forschungsgemeinschaft grant Wi 1684 is gratefully acknowledged.

References

(1) Bäckström, H. *J. Geol.* **1893**, *1*, 773–779.

(2) Spiegel, E. A. *Annu. Rev. Astro. Astrophys.* **1972**, *10*, 261–304.

(3) Gregg, M. C. *Sci. Am.* **1973**, *228*, 65–75.

(4) Bonner, F. J.; Sundelöf, L. O. *Z. Naturforsch* **1984**, *39*, 656–661.

(5) Wienken, C. J.; Baaske, P.; Rothbauer, U.; Braun, D.; Duhr, S. *Nat. Commun.* **2010**, *1*, 100.

(6) Baaske, P.; Weinert, F. M.; Duhr, S.; Lemke, K. H.; Russell, M. J.; Braun, D. *Prod. Natl. Acad. Sci. U.S.A.* **2007**, *104*, 9346–9351.

(7) Bahat, A.; Tur-Kaspa, I.; Gakamsky, A.; Giojalas, L. C.; Breitbart, H.; Eisenbach, M. *Nat. Med.* **2003**, *9*, 149–150.

(8) Budin, I.; Bruckner, R. J.; Szostak, J. W. *J. Am. Chem. Soc.* **2009**, *131*, 9628–9629.

(9) Kasparkova, V.; Halabalova, V.; Simek, L.; Ruzicka, J.; Janca, J. *J. Biochem. Biophys. Methods* **2007**, *70*, 685–687.

(10) Braun, D.; Libchaber, A. *Phys. Rev. Lett.* **2002**, *89*, 188103.

(11) Mast, C. B.; Braun, D. *Phys. Rev. Lett.* **2010**, *104*, 188102.

(12) Duhr, S.; Arduini, S.; Braun, D. *Eur. Phys. J. E* **2004**, *15*, 277–286.

(13) Duhr, S.; Braun, D. *Proc. Natl. Acad. Sci. U.S.A.* **2006**, *103*, 19678–19682.

(14) Reineck, P.; Wienken, C. J.; Braun, D. *Electrophoresis* **2010**, *31*, 279–286.

(15) Bahat, A.; Eisenbach, M. *Mol. Cell. Endocrinol.* **2006**, *252*, 115–119.

(16) Tang, J. X.; Fraden, S. *Biopolymers* **1996**, *39*, 13–22.

(17) Tang, J. X.; Fraden, S. *Liquid Crystals* **1995**, *19*, 459–467.

(18) Purdy, K. R.; Fraden, S. *Phys. Rev. E* **2004**, *70*, 061703.

(19) Barry, E.; Beller, D.; Dogic, Z. *Soft Matter* **2009**, *5*, 2563–2570.

(20) Onsager, L. *Ann. N.Y. Acad. Sci.* **1949**, *51*, 627–659.

(21) Khokhlov, A. R.; Semenov, A. N. *Physica A* **1982**, *112*, 605–614.

(22) Dogic, Z.; Philipse, A. P.; Fraden, S.; Dhont, J. K. G. *J. Chem. Phys.* **2000**, *113*, 8368–8380.

(23) Kang, K. G.; Lettinga, M. P.; Dogic, Z.; Dhont, J. K. G. *Phys. Rev. E* **2006**, *74*, 026307.

(24) Kang, K.; Dhont, J. K. G. *Eur. Phys. J. E* **2009**, *30*, 333–340.

(25) Zhang, Z.; Buitenhuis, J.; Cukkemane, A.; Brocker, M.; Bott, M.; Dhont, J. K. G. *Langmuir* **2010**, *26*, 10593–10599.

(26) Bhattacharjee, S.; Glucksman, M. J.; Makowski, L. *Biophys. J.* **1992**, *61*, 725–735.

(27) Tan, W. M.; Jelinek, R.; Opella, S. J.; Malik, P.; Terry, T. D.; Perham, R. N. *J. Mol. Biol.* **1999**, *286*, 787–796.

(28) et al., P. L. private communication.

(29) Wiegand, S.; Ning, H.; Kriegs, H. *J. Phys. Chem. B* **2007**, *111*, 14169–14174.

(30) Sambrook, J.; Russell, D. *Molecular Cloning: A Laboratory manual.*; Sold Spring Harbor laboratory Press, New York, 2001.

(31) Kang, K.; Wilk, A.; Patkowski, A.; Dhont, J. K. G. *J. Chem. Phys.* **2007**, *126*, 214501.

(32) Berkowitz, S. A.; Day, L. A. *J. Mol. Biol.* **1976**, *102*, 531–547.

(33) Thyagarajan, K.; Lallemand, P. *Opt. Commun.* **1978**, *26*, 54–57.

(34) Köhler, W. *J. Chem. Phys.* **1993**, *98*, 660–668.

(35) Köhler, W.; Rossmanith, P. *J. Phys. Chem.* **1995**, *99*, 5838–5847.

(36) Köhler, W.; Schäfer, R. In *New Developments in Polymer Analytics II*; Schmidt, M., Ed.; Advances in Polymer Science; Springer: Berlin, 2000; Vol. 151; pp 1–59.

(37) Wiegand, S.; Köhler, W. *Thermal Nonequilibrium Phenomena in Fluid Mixtures*; Springer: Berlin, 2002; Vol. LNP584; pp 189–210.

(38) Leppla, C.; Wiegand, S. *Philos. Mag* **2003**, *83*, 1989–1999.

(39) Ning, H.; Datta, S.; Sottmann, T.; Wiegand, S. *J. Phys. Chem. B* **2008**, *112*, 10927–10934.

(40) Arlt, B.; Datta, S.; Sottmann, T.; Wiegand, S. *J. Phys. Chem. B* **2010**, *114*, 2118–2123.

(41) Blanco, P.; Wiegand, S. *J. Phys. Chem. B* **2010**, *114*, 2807–2813.

(42) Blanco, P.; Kriegs, H.; Arlt, B.; Wiegand, S. *J. Phys. Chem. B* **2010**, *114*, 10740–10747.

(43) Wittko, G.; Köhler, W. *Philos. Mag.* **2003**, *83*, 1973–1987.

(44) Ning, H.; Kita, R.; Kriegs, H.; Luettmer-Strathmann, J.; Wiegand, S. *J. Phys. Chem. B* **2006**, *110*, 10746–10756.

(45) Rauch, J.; Köhler, W. *J. Chem. Phys.* **2003**, *119*, 11977–11988.

(46) Ning, H.; Buitenhuis, J.; Dhont, J. K. G.; Wiegand, S. *J. Chem. Phys.* **2006**, *125*, 204911.

(47) Dhont, J. *An introduction to Dynamics of Colloids*, 1st ed.; Studies in Interface Science; Elsevier: Amsterdam, 1996; Vol. II; p 642.

(48) Zimmermann, K.; Hagedorn, H.; Heuck, C. C.; Hinrichsen, M.; Ludwig, H. *J. Biol. Chem.* **1986**, *261*, 1653–1655.

(49) McPhie, M. G.; Nägele, G. *J. Chem. Phys.* **2007**, *127*, 034906.

(50) Nägele, G. *The physics of colloidal soft matter*; Institute of Fundamental Technological Research, Polish academy of Science: Warsaw, 2004; Vol. 14; pp 1–181.

(51) Gapinski, J.; Wilk, A.; Patkowski, A.; Häussler, W.; Banchio, A. J.; Pecora, R.; Nägele, G. *J. Chem. Phys.* **2005**, *123*, 054708.

(52) Lettinga, M. P.; Dhont, J. K. G.; Zhang, Z.; Messlinger, S.; Gompper, G. *Soft Matter* **2010**, *6*, 4556–4562.

(53) Iacopini, S.; Piazza, R. *Europhys. Lett.* **2003**, *63*, 247–253.

(54) Ning, H.; Dhont, J. K. G.; Wiegand, S. *Langmuir* **2008**, *24*, 2426–2432.

(55) Piazza, R.; Guarino, A. *Phys. Rev. Lett.* **2002**, *88*, 208302.

(56) Stadelmaier, D.; Köhler, W. *Macromolecules* **2009**, *42*, 9147–9152.

(57) Kishikawa, Y.; Wiegand, S.; Kita, R. *Biomacromolecules* **2010**, *11*, 740–747.

(58) Piazza, R.; Iacopini, S.; Triulzia, B. *Phys. Chem. Chem. Phys.* **2004**, *6*, 1616–1622.

(59) Iacopini, S.; Rusconi, R.; Piazza, R. *Eur. Phys. J. E* **2006**, *19*, 59–67.

(60) Vigolo, D.; Buzzaccaro, S.; Piazza, R. *Langmuir* **2010**, *26*, 7792–7801.

(61) Sugaya, R.; Wolf, B. A.; Kita, R. *Biomacromolecules* **2006**, *7*, 435–440.

(62) Maier, E. E.; Krause, R.; Deggelmann, M.; Hagenbuchle, M.; Weber, R.; Fraden, S. *Macromolecules* **1992**, *25*, 1125–1133.

(63) Kita, R.; Wiegand, S.; Luettmer-Strathmann, J. *J. Chem. Phys.* **2004**, *121*, 3874–3885.